Available online at www.sciencedirect.com

ScienceDirect

Geochimica et Cosmochimica Acta 307 (2021) 338–350

Geochimica et Cosmochimica Acta

www.elsevier.com/locate/gca

Response

The contribution of hydrodynamic processes to calcite dissolution rates and rate spectra

Priyanka Agrawal [a,*], Till Bollermann [b], Amir Raoof [a], Oleg Iliev [c,d], Cornelius Fischer [b], Mariëtte Wolthers [a]

[a] Department of Earth Sciences, Utrecht University, Utrecht, The Netherlands
[b] Helmholtz-Zentrum Dresden-Rossendorf, Inst. f. Ressourcenökologie, Abt. Reaktiver Transport, Leipzig, Germany
[c] Fraunhofer Institute for Industrial Mathematics ITWM, Kaiserslautern, Germany
[d] Institute of Mathematics, Bulgarian Academy of Sciences, Sofia, Bulgaria

Received 9 October 2020; accepted in revised form 2 May 2021; available online 7 May 2021

Abstract

Recent measurements on the dissolution rate of nano- and micron-scale rough calcite surfaces have shown lateral variations in dissolution rate, which can be quantified using rate spectra. This study uses numerical simulations to investigates the hydrodynamic processes during such experiments to explore whether hydrodynamic effects can explain the observed dissolution rate spectra. For this purpose, we simulated the dissolution processes of nano- and micron-scale rough calcite surfaces in COMSOL Multiphysics. We imposed surface topographies and local reaction rates measured using Vertical Scanning Interferometry (VSI), and implemented the same flow rate (i.e., 6×10^{-8} m^3 s^{-1}), solution chemistry (pH 8.8, alkalinity 4.4 meq/kg-H_2O and pCO_2 $10^{-3.48}$ bar) and flow-cell geometry as those used in the experiment. We have compared the simulated rate spectra against the experimentally measured values at a calcite surface having the same surface topography and reactive-flow conditions.

Simulations using a single dissolution rate for the rough calcite surface did not produce similarly wide dissolution rate spectra like those observed experimentally. Our results have shown that only by explicitly incorporating the rate spectra in the model the simulated and the measured rate spectra would match. Sensitivity analyses by varying chemical composition and flow velocity were performed to examine the effects of these parameters on the calculated rate spectra. This study concludes that for the reactive-flow regimes where dissolution rate spectra are observed experimentally, the chemical heterogeneity, topography of the crystal surface and the resulting heterogeneity in the free energy landscape at the surface play a major role in controlling the dissolution rate spectra. With the injection of more acidic (pH 2) solutions at higher velocities (i.e., 0.04 m s^{-1}), we observed an increase in the hydrodynamics-induced rate variability at microscopically rough surfaces.

Keywords: Calcite dissolution; Pore-scale reactive transport model; Microscopic surface experiments; Surface roughness; Hydrodynamic effects; Dissolution rate spectra

* Corresponding author.
E-mail addresses: p.agrawal@uu.nl, m.wolthers@uu.nl (P. Agrawal).

https://doi.org/10.1016/j.gca.2021.05.003
0016-7037/

1. INTRODUCTION

In past decades, numerous experiments have been conducted to better understand the controlling processes for calcite dissolution at both the macroscopic bulk scale (Plummer, 1978; Sjöberg and Rickard, 1984; Busenberg and Plummer, 1986; Chou et al., 1989; Pokrovsky et al., 2005) and at the microscopic scale (Shiraki et al., 2000; Arvidson et al., 2003; Lüttge et al., 2003; Fischer et al., 2012; Brand et al., 2017). Yet, the reported rate equations provide different surface normalized dissolution rates for similar state of the solution (i.e., similar pH, Omega, DIC) with discrepancies over several orders of magnitude (Arvidson et al., 2003, Bollermann and Fischer, 2020). Several explanations have been suggested for this discrepancy including (i) different laboratory settings leading to flow heterogeneity within the reactor, e.g. fluidized bed reactors (Chou et al., 1989) or disk-shaped flow cells (Arvidson et al., 2003) or mixed-flow reactors (Pokrovsky et al., 2005), or rotating disk batch reactors (Sjoberg and Rickard, 1984; Pokrovsky et al., 2005), (ii) the texture of the reacting substrate i.e., single crystals (Sjoberg and Rickard, 1984; Busenberg and Plummer, 1986), powder (Plummer L. N., 1978; Chou et al., 1989; Pokrovsky et al., 2005), single crystal surfaces with defect structures and variation in dissolution mechanism such as the step-wave model ((Lasaga and Luttge, 2001), and iii) the intrinsic variability of surface reactivity, expressed by dissolution rate spectra (Fischer et al., 2012; Brand et al., 2017; Noiriel et al., 2020). Mineral surface area has also been suggested as a source of uncertainty related to reasons (ii) and (iii) above, since bulk experiments rely on the value of the surface area of the substrate (crystal/powder) to calculate normalized rate values that can be compared across different investigations. Therefore, accurate parameterization of mineral surface area becomes critical. Three definitions for the surface area have been discussed in the literature including (a) geometric surface area, GSA, which assumes microscopically smooth crystal surfaces, (b) specific surface area, SSA, which corrects for smoothness assumption and takes care of surface roughness, and (c) reactive surface area, RSA, which is often related to the SSA using a constant factor often set between one and three with no clear basis for this choice (Yoon et al., 2012; Steefel et al., 2015; Yoon et al., 2015; Yoon et al., 2019).

Dissolution experiments at the microscopic scale, such as those using Atomic Force Microscopy (AFM), Vertical Scanning Interferometry (VSI) and X-ray Computer Tomography (XCT) approaches obtain dissolution rates directly from the evolution of the subsequently measured crystal surface area (Shiraki et al., 2000; Arvidson et al., 2003; Fischer et al., 2012; Brand et al., 2017). These methods capture the temporal evolution of crystal surface morphology at nano- to micro-scale without any assumptions about surface reactivity and surface area normalization via rate map measurements and calculations (Fischer et al., 2012; Emmanuel and Levenson, 2014; Yuan et al., 2019; Kahl et al., 2020; Noiriel et al., 2020). The topography evolution information combined with the molar volume of calcite dissolved provides the dissolution rate average and/or the lateral heterogeneity. In the past, such studies have revealed that the molecular-scale crystal structures, such as point defects, etch pits, steps and faces significantly influence the calcite dissolution rate and mechanism (Fischer et al., 2012; Brand et al., 2017; Noiriel et al., 2020). These studies have shown that in the case of crystal heterogeneity (particularly, crystal surface heterogeneity) a rate spectrum for the surface reactivity more adequately describes dissolution, in comparison with using a single value for the reaction rate (Fischer et al., 2012). Furthermore, molecular level modelling with kinetic Monte Carlo algorithms have shown that the kink site density, modified by both the defect density and the surface nano-topography is critically controlling the reaction kinetics, e.g., (Fischer et al., 2018; Kurganskaya and Rohlfs, 2020).

Flow-through experiments rely on certain assumptions regarding the hydrodynamic effects. A key assumption is related to the mass transfer conditions at the surface section under investigation. One of the prerequisites of AFM and VSI experiments is the prevalence of surface-controlled conditions. Constraints about fluid residence time etc. are discussed in detail in literature, exemplified by the observations on calcite surface step movement as a function of distance from equilibrium during dissolution reaction at different flow-through rates (Liang and Baer, 1997). In general, the demanded value of the flow rate emanates from a sensitivity test where the mean dissolution rate of the observed calcite surface section levels off as flow rate increases (e.g. Fig. 1 in Liang and Baer, 1997). Eventually, the onset of a steady state reaction rate, independent of flow rate, gives a cut-off flow rate above which the reactive transport system is assumed to be kinetically/surface controlled. However, several reactive transport simulations of AFM fluid cells, particularly for gypsum dissolution, have previously revealed that the transport conditions in cells are often more complex (Gasperino et al., 2006; Peruffo et al., 2016). For example, Peruffo et al (2016), inspected the impact of mass transfer conditions over the assumed kinetics-controlled reaction regime. They found that the flow rate value of 5×10^{-8} m^3 s^{-1} in a fluid cell of a volume of 100 μL produces a reaction-controlled regime, based on a sensitivity test. However, in reality this flow rate leads to a build-up of calcium and sulfate in the order of 7 mM near the gypsum surface. This indicates the prevalence of a mixed surface-transport controlled regime at higher flow rates depending on the solubility of the solid under investigation.

Surface roughness is a factor which may contribute to an enhancement of a boundary layer where dissolution products can accumulate. At the pore scale, it has been shown that the surface roughness of minerals influences the hydrodynamic interactions between fluid and solid surface through the development of the non-uniform diffusion boundary layer (DBL, Jeschke and Dreybrodt, 2002). Such a non-uniform diffusive boundary layer results into localized stagnant/immobile zones on mineral surface which attain lower values for the reaction rate. In the past, a number of pore-scale studies have explored the hydrodynamics of differently textured porous media and the effect of diffusion boundary layer development on the calcite dissolution rate (Yoon et al., 2012; Noiriel, 2015; Yoon et al., 2015;

Deng et al., 2018; Yoon et al., 2019; Molins et al., 2020). Moreover, a limited number of studies have quantified the hydrodynamics at a nano- and micron-scale rough calcite surfaces during surface dissolution experiments (Levenson and Emmanuel, 2013; Levenson et al., 2015). For example, Deng et al., 2018, presented an explicit control of the pore scale hydrodynamics for a range of transport and reaction regimes and upscaled these pore scale processes to estimate a correlation factor for the reactive and specific surface areas. However, this study utilized fracture profiles with much higher roughness magnitude (>10 μm) than the generally observed roughness magnitude of calcite surface in VSI and AFM experiments. Levenson et al. (2013), simulated the crystal surfaces obtained from AFM experiments and showed that for a given roughness magnitude of the crystal and under surface-controlled dissolution conditions, the diffusion boundary layer remains uniform. However, they also noted that the choice of the chemistry model might influence this observation. This motivates the current study to utilize a detailed reactive transport model for delineating the fluid hydrodynamics at a nano- and micron-scale rough calcite surfaces for both reaction and transport-controlled dissolution regimes.

The main goal of this paper is to examine whether the experimentally observed lateral heterogeneities in dissolution rates (rate spectra) at the microscopic scale can be explained by the contribution of hydrodynamic effects. Initially, we investigated the influence of nano to micron scale surface roughness of the crystal on the dissolution rate variability under surface-controlled regimes. For this purpose, a set of simulations, centered around the dissolution experiments from Bollermann and Fischer (2020) were carried out. These simulations were performed in COMSOL Multiphysics at the scale of the whole flow cell utilized for calcite marble dissolution experiments. These simulations were performed using a flat surface as well as using the surface topography of the VSI experiment from Bollermann and Fischer (2020) taken at a time of t = 10 hours. Each of these dissolution simulations were performed using either a single rate or a rate spectrum. In all simulations, the bottom surface of the flow cell was a single grain calcite surface. Next, in order to get further insight into the impact of nano or micron scale surface roughness on the dissolution rate variability under transport-controlled regimes, sensitivity studies were performed by varying chemical composition and flow velocity in smaller-scale simulations and using higher numerical resolution. In summary, this study aims to answer whether hydrodynamic effects or the calcite surface topography, or their coupled interaction, can explain the observations of surface-direct measurements of dissolution rate spectra.

2. MATERIALS AND METHODS

In this study, centimeter to millimeter scale reactive transport including single-phase fluid flow, transport of the multiple solute species, and chemical reactions were simulated in the presence of nano- and micron-scale roughness of the calcite crystal surface by solving a coupled system of non-linear equations in 3D model set-up using COMSOL Multiphysics. The following subsections provide the modelling formulation. Further details of the numerical method can be found in (Agrawal et al., 2020).

2.1. Fluid flow and transport

To simulate fluid flow, we have considered laminar flow (i.e., resulting in a Reynolds number Re < 100) and incompressible fluid in Navier - Stokes equations to obtain:

$$\rho\left(\frac{\partial u}{\partial t}+u.\nabla u\right)=-\nabla p+\mu\nabla^2 u \tag{1}$$

$$\nabla.u=0 \tag{2}$$

where p is pressure, u is velocity, ρ is the fluid density and μ is the fluid viscosity. Initially, i.e., at the time of zero, steady state flow field conditions were maintained in the domain. Further details on the boundary conditions are provided in SI Section S1.1.

Transport of the aqueous species was modelled using the advection–diffusion-reaction equation complemented with an extra term to represent chemical reactions as:

$$\frac{\partial c_i}{\partial t}+\nabla.(-D.\nabla c_i)+\nabla.(u.c_i)=R_i \tag{3}$$

where, D is the diffusion coefficient taken as 3.36×10^{-9} ($m^2\ s^{-1}$), c_i and R_i are concentration (mol m^{-3}) and reaction input of i^{th} species (mol $m^{-3}\ s^{-1}$), respectively.

Transport of mass in normall direction to the calcite surface was used to represent calcite dissolution at the fluid–solid boundary as:

$$-n.(-D.\nabla c_i+u.c_i)=R_{Calcite} \tag{4}$$

where, $R_{Calcite}$ (mol $m^{-2}\ s^1$) is the calcite dissolution rate calculated from Eq. (5). Further details on the boundary conditions are provided in SI Section S1.1.

In order to investigate the coupling of flow and reactive transport during the transient stage (i.e., before that the simulations show a steady-state behavior), we simulated time-dependent forms of flow and transport equations.

2.2. Geochemical model

The aqueous complexation reactions corresponding to the dissolution of CO_2 in the water were implemented as equilibrium reactions, i.e., they were assumed to occur instantaneously, which under the simulated conditions may be considered a valid approximation (Zeebe and Wolf-Gladrow, 2001). Table 1 provides chemical reactions together with the corresponding equilibrium constant values.

Dissolution of calcite can be simulated by applying three pathways (Plummer et al., 1978; see details in SI Section S1.2) rates of which can be combined into a single dissolution rate law as:

$$R_{Calcite}[\mathrm{molm^{-2}S^{-1}}]=R_I R_E \tag{5}$$

$$R_E[\mathrm{molm^{-2}S^{-1}}] = (k_1 a_{H^+} + k_2 a_{CO_2(aq)} + k_3 a_{H_2O}) \times (1 - 10^{0.67SI}) \quad (6)$$

where R_I denotes the intrinsic rate factor derived from molecular scale roughness of the calcite surface (Fischer et al., 2012), R_E is the extrinsic rate factor derived from the composition of the solution. SI is the saturation index of the solution calculated as $(a_{Ca^{2+}} a_{CO_3^{2-}})/(K_{eq})$, where $K_{eq} = 10^{-8.48}$ (Plummer and Busenberg, 1982). a_i is the activity of the i^{th} species calculated from the concentration of the i^{th} species and ionic strength of the solution using Davies equation. In Eq. Eqn 6, the first term represents the driving force while the second term determines the distance from the equilibrium state. All chemical reactions were implemented in the COMSOL model and solved simultaneously as a fully coupled system.

For this study, we implemented four types of calcite dissolution rate models through variations in R_I. In the first type, the reactivity of the calcite surface was assumed to be controlled only by the composition of the solution and therefore the value of R_I was set to 1. Models with a single value of R_I include 1R in the nomenclature (Table 2). The remaining three types of models included location dependent values for R_I– i.e., $R1_I(x1, y1)$, $R2_I(x2, y2)$ and $R3_I(x3, y3)$. To calculate these values, three areas of size 0.021×0.021 mm^2 were extracted from different regions of a reaction rate map obtained experimentally in a VSI setup (Fig. S2). This reaction rate map was obtained using a dissolution time frame taken from time periods of 2–6 hours. For more information on the reaction rate map see (Bollermann and Fischer, 2020). Calculation of $R_I(x, y)$ was performed as:

Table 1
Implemented bulk phase reactions and their corresponding equilibrium rate constants.

Reactions	Equilibrium rate constant
$CO_2(aq) = H^+ + HCO_3^-$	[a] 4.5×10^{-7}
$HCO_3^- = H^+ + CO_3^{2-}$	[a] 4.78×10^{-11}
$H_2O = H^+ + OH^-$	1×10^{-14}

[a] Equilibrium rate constants were taken from Plummer and Busenberg (1982).

$$R_I(x, y) = \frac{R_{VSI}(x, y)}{R_{VSI,m}} \quad (7)$$

where, $R_{VSI}(x, y)$ is the reaction rate recorded in VSI experiment and $R_{VSI,m}$ is the mode of the $R_{VSI}(x, y)$ of the extracted area. Models with location specific value of $R1_I(x1, y1)$, $R2_I(x2, y2)$ and $R3_I(x3, y3)$ include RS1, RS2 and RS3, respectively, in the nomenclature (Table 2).

2.3. Physical-chemical parameters

2.3.1. Numerical models of physical domains/geometry

Two numerical models of physical domains were utilized in the current study as base models. *Set I* is geometrically identical to a flow cell used to perform calcite marble dissolution experiments in Bollermann and Fischer (2020). Simulation conditions including flow rate and solution compositions were chosen to represent the conditions of the experimentally measured surface roughness and dissolution rate spectra (Bollermann and Fischer, 2020). This base model and its variations (Table 2) was aimed at studying different surface topographies and different kinetics of the dissolution processes (Fig. S3).

Set II is a small parallelepiped sub-volume taken from the larger *set I* domain, requiring relatively less computational time than *set I*. *Set II* consists of two variants (Table 3), which were used in parametric and sensitivity studies of dissolution processes under different flow rate and solution composition. Figs. S2 and S3 provide conceptual pictures of all the variants of *Model G1-Flat-1R* and *Model G2-Flat-1R*. A more detailed description of the considered numerical models/geometries reads as follows.

Set I.

Model G1-Flat-1R represents the whole disk-shaped flow cell with a diameter of 15 mm and a thickness value of 1.75 mm as shown in Fig. 1, with an entirely flat surface and single dissolution rate imposed in the simulation. A single grained calcite surface served as the base surface of the flow cell. In the VSI experiment, calcite marble was the investigated polycrystalline material, part of which was masked using an inert material (with thickness ~ 550 nm) so that it could be used as the reference point after the experiments. Further details regarding the experimental setup are available in Bollermann and Fischer (2020). *Model G1-Flat-1R* included all these settings to be consis-

Table 2
Variants of *set I*, the base Model G1 i.e., Full 3D flow cell for calcite marble dissolution experiment used in this study and their main properties. [1]topography h1(x1, y1), [2]topography h2(x2, y2) and [3]topography h3(x3, y3) from (Bollermann and Fischer, 2020); [4] $R_I = R1_I(x1, y1)$ in Eq. (5); [5] $R_I = R2_I(x2, y2)$ in Equation (5); [6] $R_I = R3_I(x3, y3)$ in Eq. (5) from (Bollermann and Fischer, 2020).

Model	Highlight surface	Kinetics
Model G1-Flat-1R	Flat reactive surface	Single value of $\boldsymbol{R_I}$ in Eq. (5)
Model G1A-HE1-1R	Area *A:* topography and height from experiment[1]	Single value of $\boldsymbol{R_I}$ in Eq. (5)
Model G1A-HE2-1R	Area *A:* topography and height from experiment[2]	Single value of $\boldsymbol{R_I}$ in Eq. (5)
Model G1A-HE3-1R	Area *A:* topography and height from experiment[3]	Single value of $\boldsymbol{R_I}$ in Eq. (5)
Model G1A-HE1-RS1	Area *A:* topography and height from experiment[1]	Location specific values of $\boldsymbol{R1_I}$[4] in Eq. (5)
Model G1A-HE2-RS2	Area *A:* topography and height from experiment[2]	Location specific values of $\boldsymbol{R2_I}$[5] in Eq. (5)
Model G1A-HE3-RS3	Area *A:* topography and height from experiment[3]	Location specific values of $\boldsymbol{R3_I}$[6] in Eq. (5)

Table 3
Variants of the base *Model G2* i.e., small 3D parallelepiped used in this study and their main properties. [1]topography $h1(x1, y1)$ from (Bollermann and Fischer, 2020).

Model	Highlight surface	Kinetics
Model G2 – Flat-1R	Flat reactive surface	Single value of $\boldsymbol{R_I}$ in Eq. (5)
Model G2 – HE1-1R	*Area A''* : topography and height from experiment[1]	Single value of $\boldsymbol{R_I}$ in Eq. (5)

tent with the experiments, except for the surface topography. Furthermore, for result analysis, we have chosen an area with a size of 0.021 × 0.021 mm^2 on the surface of the crystal, namely *area* A. The location of the *area* A is shown in Fig. 1. From the VSI experiment we obtained point wise height and reaction rate information of the calcite marble surface which was imposed at the single grain calcite surface of area *A*. A smooth surface was used to fit to these points and was meshed using tetrahedral mesh elements. A high resolution (0.4 μm size of tetrahedral mesh elements) for the surface topography was used for area *A* in all G1 variants and a low resolution (0.23 mm size of triangular mesh elements) was used in the remaining parts of the flow cell.

Six variants of *Model G1-Flat-1R* were considered to investigate the influence of experimentally measured crystal surface topography and the kinetics of the dissolution process (Table 2, HE in nomenclature corresponds to the crystal surface topography). In some of the HE models, location specific values of R_I (i.e., $R1_I(x1, y1)$, $R2_I(x2, y2), R3_I(x3, y3)$) were implemented (see Section 2.1.2 for more details).

Set II

For the sensitivity analyses presented in Sections 3.3, *Model G2–Flat-1R*, was developed. This model contained a rectangular flow domain with a dimension of 1 mm (length) × 0.3 mm (width) × 1.75 mm (depth). At 0.8 mm from the inlet boundary and 0.13 mm from the lateral boundary of the domain, *Area A''* (0.021 × 0.021 mm^2) was either kept as flat surface (*Model G2–Flat-1R*) or replaced with the same experimental topography as in *Model G1A-HE1-1R* (*Model G2A'' – HE1-1R*) (Fig. S4). Boundary conditions were set to ascertain that *Area A''* in *Model G2–Flat-1R* has similar flow conditions as *Area A* in *Model G1-Flat-1R*.

2.3.2. Chemical compositions and flow rates

For this study, five sets of injecting solutions with different compositions, Sol. #1, Sol. #2, Sol. #3, Sol. #4, Sol. #5, were considered. Sol. #1 (i.e., pH 8.8 and alkalinity of 4.4 meq/kg-H_2O) was similar to the solution used in the VSI experiments from which the topography and dissolution rate maps were obtained for our models, except the added amount of Ca^{2+} species with an amount of 1×10^{-6} mol m^{-3} (as explained in Fig. S1). The composition of all inflow solutions with target pH values and pCO_2 conditions were initially defined using PhreeqC program (Parkhurst and Appelo, 2013) with the phreeqc.dat database. Except Sol. #2, all other solutions were prepared for a system open to the atmospheric. The choice of simulating an open system is due to the experimental conditions we aim to simulate. In those experiments, solutions that were initially in equilibrium with atmospheric CO_2 were injected in the flow cell. The corresponding values of the species concentrations in the inflow solutions are provided in Table S1. Note that the current model did not simulate ions pairs of Ca^{2+} such as $CaCO_3$ and $CaHCO_3^-$. This consideration will have an impact on the absolute dissolution rates, but we assume that its impact on the width of the dissolution rate spectra is negligible.

In all models, the flow cell was considered to be filled with the injecting solution at the beginning of the simulation. The imposed values of flow rate and average velocity are provided in Tables S2 and S3. Note that all the above simulation conditions were selected based on the calcite dissolution experiments to which our simulations compare and other comparable, commonly conducted experiments, i.e., dissolution experiments using nano- and micron-scale rough calcite surfaces.

2.4. Parametrization of the flow and reaction regimes

The Péclet number, *Pe*, is defined as:

$$Pe = \frac{vh}{D} \tag{8}$$

where v is the location specific average velocity, h is the height of the investigated volume (disk or rectangle, depending on the model run).

For the investigated systems, we defined two Damköhler numbers. The first Damköhler number, Da_I, compared the reaction time scale with the diffusion time scale as:

$$Da_I = \frac{h^2 * S_R}{D * C_{Calcite}} \tag{9}$$

$C_{Calcite}$ is the density of surface sites of calcite at the start of dissolution (mol m^{-2}) i.e., 0.8×10^{-5} mol m^{-2}. S_R is the mean dissolution rate (mol m^{-2} s^{-1}) calculated from observed reaction rates at a surface of size (0.021 × 0.021 mm^2) i.e., Area *A* in *Model G1-Flat-1R*. and Area *A''* in *Model G2–Flat-1R*; unless otherwise noted. Mean dissolution rate was calculated as:

$$S_R = \frac{\sum_{i=1}^{N_i} R_{Calcite}(x, y)}{N_i} \tag{10}$$

where N_i is the total numbers of grid points from which dissolution rate was utilized in calculation. In a surface size of 0.021 × 0.021 mm^2, a total of 144 grid points were utilized such that the distance between each grid point was 0.148×10^{-3} mm.

The second Damköhler number, Da_{II}, compared the reaction time scale with the advection time scale as:

$$Da_{II} = \frac{h * S_R}{v * C_{Calcite}} \quad (11)$$

Tables S2 and S3 provides the Pe, Da_I and Da_{II} numbers at the examined locations in *Model G1* and *Model G2*, respectively.

3. RESULTS

Section 3.1 addresses the hydrodynamic effects and dissolution rate heterogeneity at the scale of flow cell and gives insight into the conditions under which the VSI experiments were carried out. Section 3.2 addresses the results related to the main objective of this study i.e., investigating the contribution of heterogeneity in hydrodynamics due to nano- and micron-scale surface roughness towards dissolution rate spectra. Finally, Section 3.3 investigates the impact of surface roughness on the dissolution rate variability under transport-controlled regimes.

3.1. Hydrodynamics and calcite dissolution rates at the flow-cell scale

The velocity field inside the flow cell is shown in Fig. 1. This velocity field corresponds to the flow rate of 6×10^{-8} $m^3\ s^{-1}$, which falls in the range of flow rates usually chosen for surface dissolution experiments (cf. Bollermann and Fischer, 2020). Pe and Da numbers of this numerical experiment are provided in Table S2. The heterogeneity in the velocity field was evident in a horizontal cross-section located at a height of 100 μm from the bottom surface of the cell and varied up to one order of magnitude i.e., between 1×10^{-4} (dark read, at the center) and 1×10^{-5} $m\ s^{-1}$ (dark blue, at the rims of the flow cell) (Fig. 1). All these velocities yielded low Reynolds number, thus laminar flow, while the flow streamlines showed the development of horizontal vorticity in the flow field.

The breakthrough curve of the Ca^{2+} species showed that the reactive system attained a quasi-steady state within 100 seconds of the dissolution period (Fig. S5). Fig. 2 shows the observed spatial distribution of Ca^{2+} concentration, Ω ($\Omega = 10^{SI}$ and reflects the saturation state of the solution with respect to calcite) and reaction rate at the calcite surface, after 200 s (so, after100 s quasi-steady state dissolution) in *Model G1-Flat-1R* with Sol. #1 (pH 8.8 and alkalinity of 4.4 meq/kg-H_2O).

The Ca^{2+} concentration field reflected the heterogeneity of the flow regime (Fig. 2a). For example, the high velocity belt between inlet and outlet accumulated the lowest amount of Ca^{2+} ions near the calcite surface. Contrastingly, the low velocity zones towards the boundary of the flow cell and on both sides of the high velocity belt (highlighted in the Fig. 1), showed a significantly higher accumulation of Ca^{2+} ions near the calcite surface. Despite such significant accumulation of the Ca^{2+} ions, the composition of solution away from calcite surface remained unaffected (vertical 2D slices in Fig. 2a and 2b), resulting in a significant concentration gradient in the transversal direction. This build-up of Ca^{2+} ions near the calcite surface changed the saturation state of the fluid that is in contact with the calcite surface (Fig. 2b). Such a build-up of Ca^{2+} ions at the calcite surface indicated a horizontal heterogeneity of the flow regime. Consequently, at the scale of flow cell, the developed flow and concentration heterogeneity led to an order of magnitude heterogeneity in the dissolution rate such that the zones with high dissolution rates overlapped with the high velocity regions (Fig. 2c).

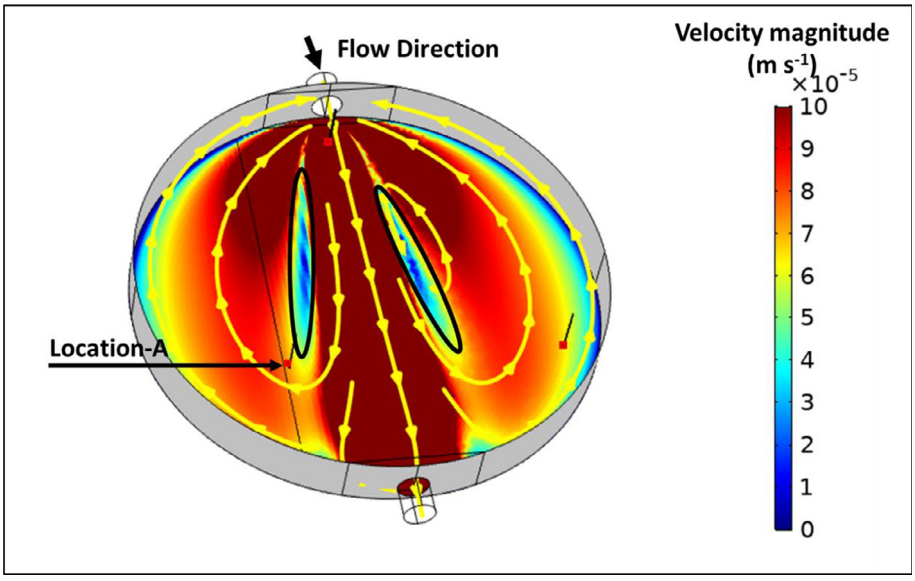

Fig. 1. The simulated domain for the whole disk-shaped flow cell, with 15 *mm* diameter and 1.75 *mm* thickness, showing the velocity field and flow streamlines at a planar surface positioned at a distance of 100 μm from the bottom of the flow cell. Regions where the magnitude of the velocity was lower than the surrounding locations are marked using black outlines.

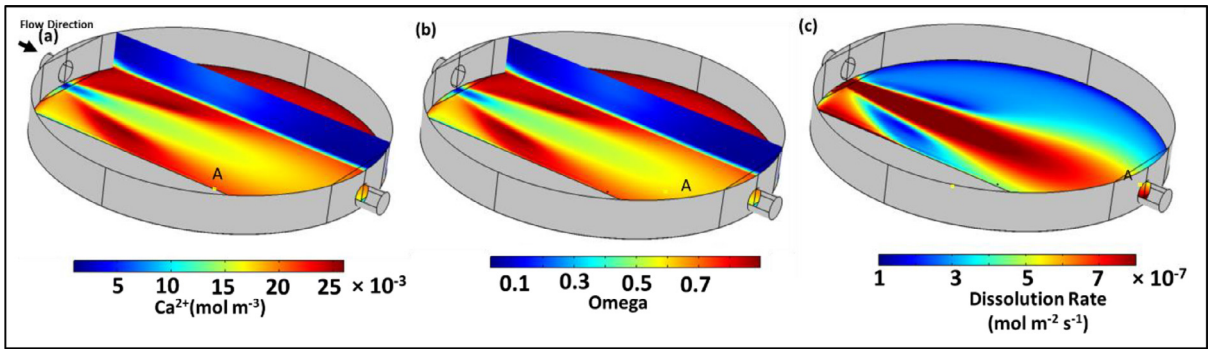

Fig. 2. The simulated flow cell showing steady state fields at the calcite surface for (a) Ca^{2+} concentration (b) saturation state of solution with respect to calcite ($\Omega = 10^{SI}$); (c) computed surface reaction rate map based on Eq. (5) at the calcite surface. Vertical 2D slices in plots a-b show vertical profiles of the respective variables. Simulation conditions are 6×10^{-8} m^3 s^{-1} flow rate, Sol. #1 (pH 8.8 and alkalinity of 4.4 meq/kg-H_2O).

We observed that the mean dissolution rate of the whole calcite surface in the flow cell was around 5×10^{-7} mol m^2 s^{-1} which is nearly one order of magnitude lower than the expected dissolution rate as per the composition of the injected solution i.e., 2.3×10^{-6} mol m^{-2} s^{-1} (Fig. 2c). The sensitivity of this rate heterogeneity towards imposed flow and reaction regime is explored further in SI Section 2. We have observed that at the scale of the observation window for the VSI experiment there was no significant composition heterogeneities around *Area A* (Fig. S9).

3.2. The rough calcite surface

In order to unravel the impact of hydrodynamics near rough surfaces on measured dissolution rates, we focus on area *A* (Fig. 1), which is of similar size to the field of view used in VSI experiments that revealed the surface topography variability and dissolution rate spectra. Simulations were performed with experimental solution pH (8.8, Sol. #1) and flow rate (6×10^{-8} m^3 s^{-1}; Pe and Da numbers of this numerical experiment are provided in Table S2).

Reaction rate maps were obtained for location A with a smooth surface (*Model G1-Flat-1R*) as well as with the VSI experiment-based topography (*Model G1A-HE1-1R*) imposed (Fig. 3a and b). When location A was flat, a constant solution composition (i.e., no horizontal gradient) was observed at steady state, resulting in a homogenous constant dissolution rate of 4.69×10^{-7} mol m^{-2} s^{-1} (Fig. 3a). Imposition of surface topography in location A introduced heterogeneity in the flow field and concentration

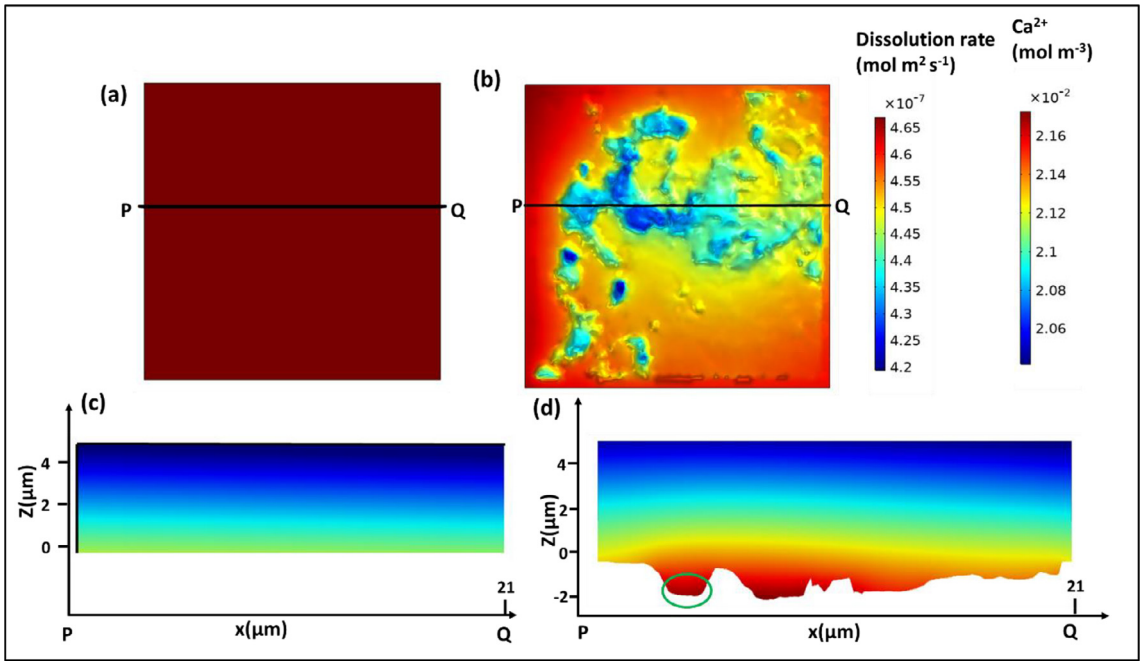

Fig. 3. Reaction rate maps of area *A*, after 200 s of solution injection using **(a)** *Model G1-Flat-1R* **(b)** *Model G1A-HE1-1R*. Vertical concentration slices of Ca^{2+} were extracted along profile PQ from **(c)** *Model G1-Flat-1R* **(d)** *Model G1A-HE1-1R*. The green color marked zone highlights Ca^{2+} enriched pockets. Simulations performed with a flow rate of 6×10^{-8} m^3 s^{-1} and using Sol. #1 (pH 8.8 and alkalinity of 4.4 meq/kg-H_2O).

field and therefore also in the reaction rates (Fig. 3b). As a result, a 4 % lower mean ± 2σ dissolution rate of 4.52 ± 0.16 × 10^{-7} mol m^{-2} s^{-1} was obtained (Fig. 3b). Fig. 3c and 3d show vertical slices with the Ca^{2+} concentration in the first 5 μm above the rough calcite surface, along the cross-section PQ shown in Fig. 3b. While the smooth calcite surface resulted in homogeneous accumulation of the Ca^{2+} concentration, the deeper (etch pit) parts at the rough calcite surface were found to be enriched in Ca^{2+} (Fig. 3c and 3d). Expectedly, due to this accumulation of Ca^{2+}, the etch pits showed lower dissolution rates (Fig. 3b) and a general depth dependency of dissolution rate was observed (see Fig. S10 and the detailed description in SI Section S3) from which the rate spectra were calculated.

The rate spectrum observed in the simulations of the rough calcite surface falls within the experimental rate spectra (Fig. 4) but shows a narrower range. The rate spectrum obtained from the simulations varied within a factor of two (Fig. 4), while the rate spectrum measured experimentally showed more than two orders of magnitude variation i.e., mean ± 2σ dissolution rate is 4.56 ± 5.56 × 10^{-7} mol m^{-2} s^{-1}.

We observed a similarly narrow spectrum when simulating two other experiment topographies (*Model G1-HE2-1R* and *Model G1-HE2-1R)*. Even amplifying the surface topography did not yield dissolution rate spectra at quasi steady state to an extent that reproduce the experimentally observed rate spectra (Fig. S11, SI Section S4)

Recall that in these simulations (*Model G1-HE1-1R, Model G1-HE2-1R* and *Model G1-HE2-1R*) a single dissolution rate was imposed, irrespective of the surface topography. In order to represent surface-controlled heterogeneity in dissolution rates, we also utilized a model in which we imposed location specific values of R_l to area A (*Model G1A- HE1-RS1*). While the *Model G1-Flat-1R* yielded a single dissolution rate and *Model G1A-HE1-1R* a very narrow dissolution spectrum in the quasi-steady state*, Model G1A-HE1-RS1* showed a wider dissolution rate spectrum with an optimum width comparable to the dissolution rate spectrum measured experimentally (Fig. 4, yellow and green line). The rate spectrum obtained from the simulations with imposed rate spectra extends over more than one orders of magnitude, similar to the rate spectrum measured experimentally. Additionally, we imposed the rate spectra extracted from two other locations in *Model G1A- HE2-RS2* and *Model G1A- HE3-RS3* and compared the simulated rate spectra with experimental rate spectra at these locations. We observed that experimental rate spectra were unique to the location of extraction (Figs. 4 and 5) and that the simulated rate spectra were of comparable width, however with a faster mean dissolution rate (Fig. 5).

3.3. Varying reaction and flow regime

To investigate the impact of flow and reaction regimes on the observed dissolution rate variability, we performed a series of simulations on smaller domain sizes using the smaller *Set II*, namely, *Model G2-Flat-1R and Model G2-HE1-1R* which are parallelepiped sub-volumes of *Model G1-Flat-1R* (Fig. S4).

For a given flow velocity, lowering the pH value of the injecting solution resulted into increased reactivity towards the calcite surface and thus increased production of the reaction products. As a result, the rate of removal of these products became the limiting factor in determining the dissolution rate and the reaction regime moved towards transport-controlled kinetics. For example, injection of a solution with a pH value of 2 at an average velocity of 0.002 m s^{-1} resulted in a mean ± 2σ dissolution rate at quasi steady state of an order of 1.10 ± 0.07 × 10^{-4} mol m^2 s^{-1} (*Model G2-HE-1R*). Due to the transport-controlled kinetics, the pH of the solution in the diffusive boundary layer was around 2.8 and little higher in the deeper etch pits (Fig. 6b). Ca^{2+} accumulation was also observed in the deeper parts of the surface profile. As a result, these etch pits attained up to 12 % lower dissolution rate (Fig. 6a) than the average dissolution rate. This decrease in the dissolution rate due to a change in reaction

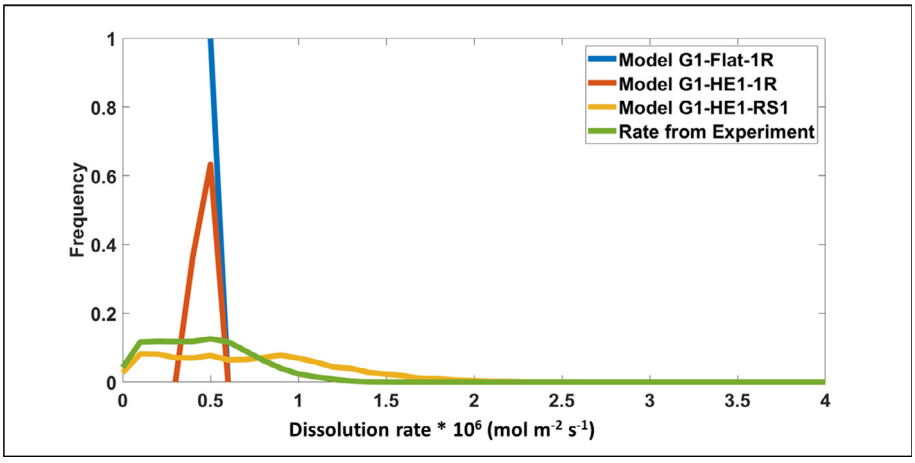

Fig. 4. Comparison of the simulated rate spectra against the experimentally observed rate spectra corresponding to surface topography $h1(x1, y1)$ and reaction rate map $R1_l(x1, y1)$. Simulation conditions included a flow rate of 6 × 10^{-8} m^3 s^{-1} using Sol. #1 (pH 8.8 and alkalinity of 4.4 meq/kg-H_2O).

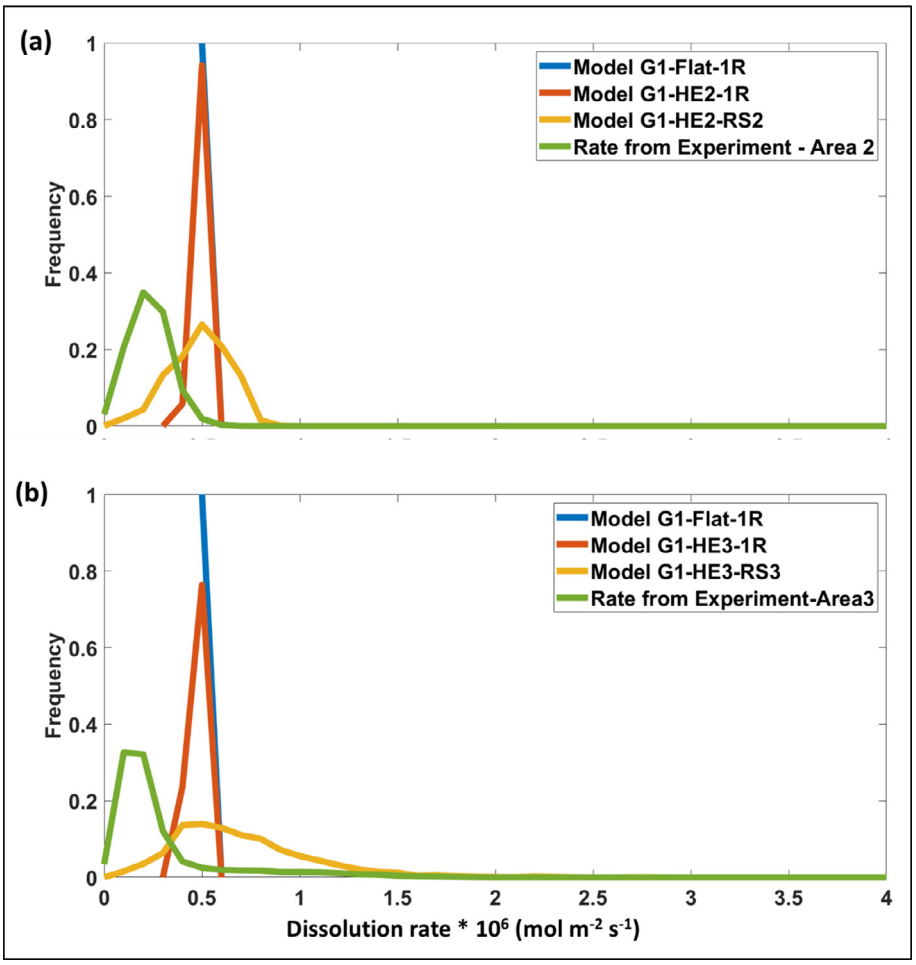

Fig. 5. Comparison of the simulated rate spectra against the experimentally observed rate spectra corresponding to (a) surface topography $h2(x2, y2)$ and reaction rate map $R2_I(x2, y2)$ and (b) surface topography $h3(x3, y3)$ and reaction rate map $R3_I(x3, y3)$. Simulation conditions included a flow rate of 6×10^{-8} m^3 s^{-1} using Sol. #1 (pH 8.8 and alkalinity of 4.4 meq/kg-H_2O).

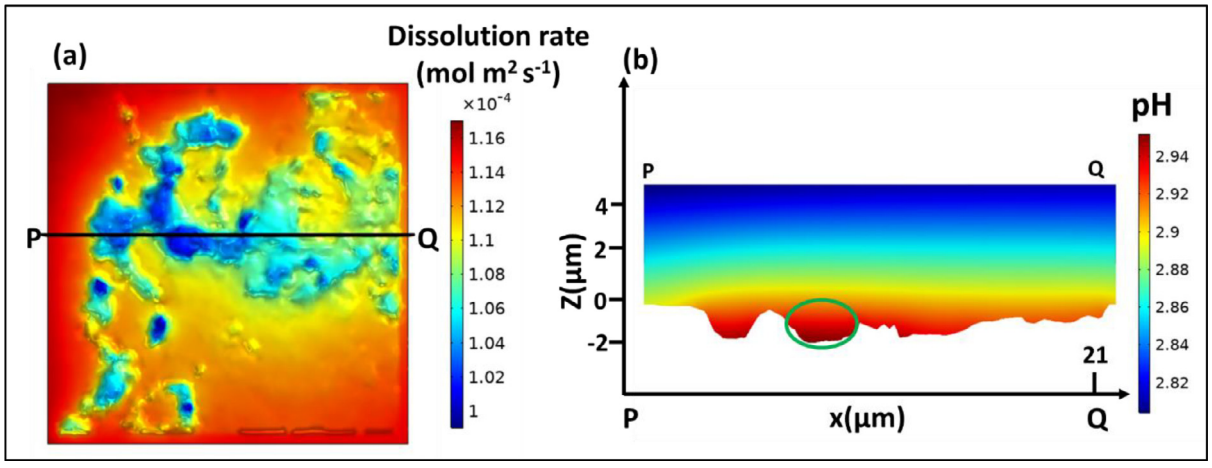

Fig. 6. **(a)** Steady state reaction rate map in location *A*" in *Model G2-HE1-1R* **(b)** Vertical concentration slice for pH obtained along profile PQ. Green oval points to the less acidic pockets. Simulation conditions were 0.002 m s^{-1} average velocity using Sol. #4 (pH 2).

regime was reflected through the increasing value of the Da number (Table S3). Calculation of the Da_I and Da_{II} number based on the steady-state mean dissolution rate (Eqs. (9) and (11)), instead of based on the composition of the injected solution, allowed for analysis of rate heterogeneity due to local factors only (such as local surface topography) independent of other factors that affect this rate (e.g. size and shape of the numerical flow cell and location of the studied area with respect to the inlet). We observed the highest heterogeneity in dissolution rates (±12 %, due only to hydrodynamics) for the given surface roughness atDa_I = 12572 (i.e., pH 2 Sol. #4) and further increase of Da_I number (i.e., decrease in pH) did not increase the rate heterogeneity any further (Figs. 7 and S12).

For the inflow solutions that were closer to equilibrium with respect to calcite, the relationship between flow rate, solution reactivity and dissolution rate heterogeneity became more complex: we observed a higher amount of rate heterogeneity for solutions with lower reactivity regimes (Fig. 7a). When the dissolution reaction time scale was 3 orders of magnitude higher than the diffusion time scale, further increase in the reactivity by lowering pH did not impact the rate heterogeneity (Fig. 7b). Contrastingly, when reaction time scales were less than 3 orders of magnitude higher than diffusion time scale, increased rate heterogeneity was observed with decreasing pH (Fig. 7). This range of Da_I number covered the state of solutions from being transport controlled (pH > 5) to surface controlled kinetics (pH < 5) (Table S3).

4. DISCUSSION

4.1. Controls on dissolution rate heterogeneity at the microscopic scale

At the microscopic scale, i.e., the scale of commonly utilized fields of view for dissolution experiments using VSI or AFM, the solution near the calcite surface was well-mixed thus a single dissolution rate was observed (Location A Fig. 3a and S9) and no impact of the flow-cell-scale rate heterogeneity was observed. Furthermore, the imposition of the real crystal topographies (Figs. 4 and 5) resulted in the development of narrow rate spectra. These rate spectra were a direct consequence of the surface roughness on local

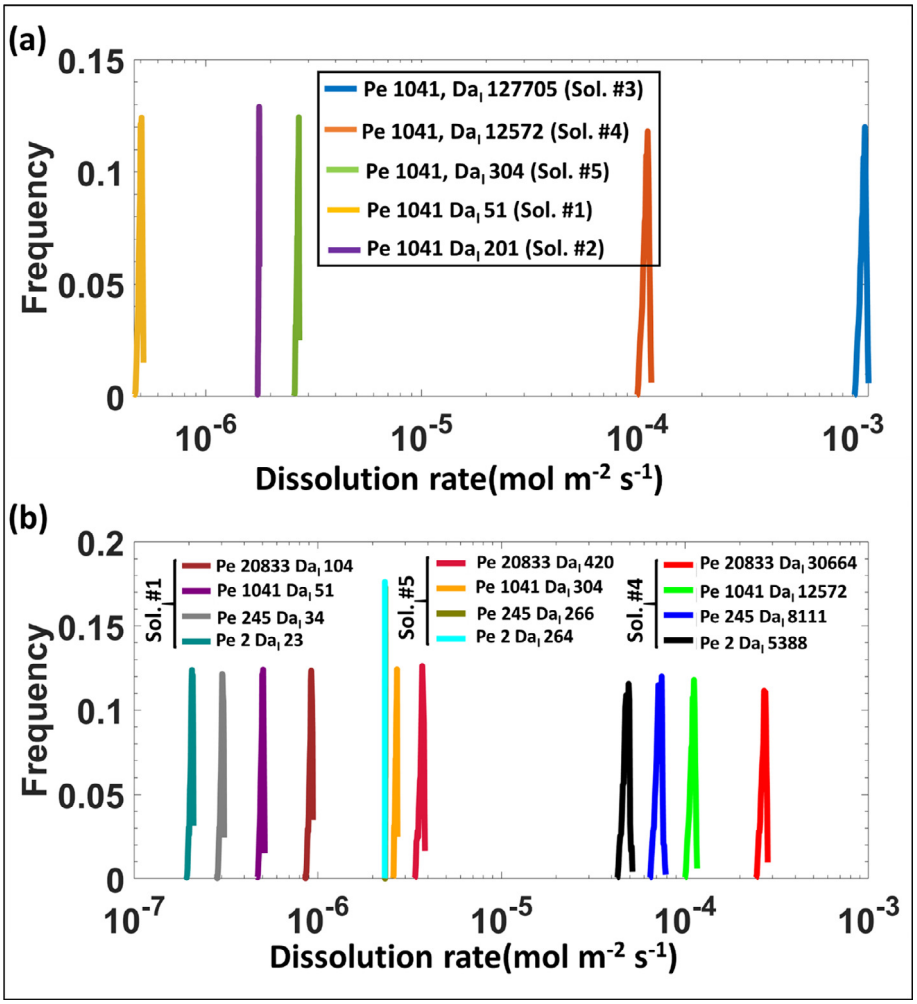

Fig. 7. Rate spectra for simulations corresponding to **(a)** fixed Pe number and different Da_I numbers, and **(b)** different Pe numbers corresponding to Da_I numbers.

hydrodynamics, since in these models (i.e., *Model G1A-HE1-1R*, *Model G1-HE2-1R and Model G1-HE3-1R*) a single reaction rate law was implemented. The observed rate spectra at the nano- and micron-scale rough calcite surface were much narrower compared to the experimentally observed rate spectra (Figs. 4 and 5). This indicates that the hydrodynamic effects created due to surface roughness are not sufficient to explain the overall experimentally observed dissolution rate heterogeneity, even until 10 hours of dissolution when deeper etch pits had evolved. In our simulations, the magnitude of roughness induced in this dissolution period did not develop significant non-uniformity in the diffusive boundary layer. Consequently, for the considered roughness and flow regime, the diffuse boundary layer can be considered of a uniform thickness. This confirms that under surface-controlled dissolution conditions, the experimentally observed rate spectra cannot be explained purely by heterogeneity in hydrodynamics induced by surface topography. The fact that we could not obtain similarly wide rate spectra without imposing rate spectra from the start of the simulations is a strong indication that calcite surfaces intrinsically show local variability in dissolution rate. These findings are in the agreement with the observation made by Levenson et al. (2013) for surface-controlled kinetics.

Such rate spectra can therefore be attributed to atomic-scale surface heterogeneities such as surface nanotopography, kink densities and defect distribution at or near the crystal surface, which result in a free-energy landscape at the dissolving surface (Shiraki et al., 2000; Arvidson et al., 2003; Lüttge et al., 2003; Fischer et al., 2012; Wolthers et al., 2012; Brand et al., 2017; De La Pierre et al., 2017).

When simulating different imposed surface topographies with the imposed rate spectra of location A, disagreement between measured and simulated rate spectra was observed (Fig. 5). This indicates that rate spectra are linked to the local surface topography and cannot be captured using a single rate spectrum. As explained in Bollermann and Fischer (2020), the investigated polycrystalline material in the VSI experiment showed additional variability in surface reactivity, e.g., due to effects of crystal orientation and twinning. Thus, the observed rate ranges are more heterogeneous than for a single crystal surface. Consequently, inclusion of rate variability in reactive transport models becomes additionally a function of the lateral variability of surface roughness, and a single rate spectrum is not sufficient to capture the rate heterogeneity of the entire surface.

4.2. Sensitivity analysis

The sensitivity analysis performed for a range of transport and reaction regimes showed that the hydrodynamics induced rate heterogeneity became more pronounced with increasing acidity of the injected solution and with increasing injection fluid velocity (Figs. 7 and S12). For the simulated roughness magnitudes of nano or micron scale, we observed that the highest noted variability in the dissolution rate due to hydrodynamics was only around 12%. This highest limit of rate heterogeneity due to hydrodynamics at the calcite surface was lower than the observed impact for the much higher roughness of a fracture (Deng et al., 2018) where the roughness was of (>10 μm) higher magnitude.

4.3. Implications

Our simulation results show that for the reactive flow regimes considered here and at the microscopic scale, surface-controlled calcite dissolution of a polycrystalline material cannot be described by a single rate law. Even a fairly flat crystal surface with nano-to-micro topography that would not yield lateral variability in dissolution rate due to the hydrodynamics effects shows a dissolution rate spectrum. Moreover, the dissolution rate spectrum varies with surface topography and the underlying crystal structure variations, increasing the variability of calcite dissolution.

At surface-controlled dissolution conditions, our results imply that

- the single rate dissolution models are not always applicable,
- as long as the rate spectra cannot be explained by hydrodynamics effects, explanations of the rate spectra phenomenon should be sought in the surface free energy landscape. Works in this area are carried out only at atomistic level, e.g., using kinetic Monte Carlo algorithms, and targeted research should be dedicated to investigating rate spectrum phenomena at larger scales.

Our sensitivity study reveals that the impact of the surface free energy landscape on the dissolution rate spectra decreases when the system moves from surface-controlled to transport-controlled conditions. This implies that

- in this case the rate heterogeneity averages out faster in space and in time, and averaged single rates can be used at larger scales. Further investigations are needed to gain qualitative and quantitative understanding of how the interactions of the local Peclet and Damköhler numbers with the crystal heterogeneity influence the applicability of averaged single rate models.
- Further investigations are needed to gain understanding on the dissolution rate spectrum phenomenon in the case of multigrain crystals in particular, and multigrain polymineral rocks in general.

5. SUMMARY AND CONCLUSIONS

1. Computer simulations of calcite marble dissolution experiments were performed at the scale of an entire flow-through cell with a fixed calcite surface

as its base. Significant lateral heterogeneity of the flow and the concentration within the considered flow cell was observed. Together with the developed vertical diffusion layer, these variations led to considerable discrepancy between the reactivity calculated using the mass outflow from the flow cell using the composition of the injected fluid, and the real local reactivities within the flow cell. However, at the small scale within the observation area of, for example, AFM or VSI measurements, the horizontal heterogeneity of the fluid composition was negligible.

2. The simulations at conditions corresponding to the reaction and flow regime of VSI surface dissolution experiment by Bollermann and Fischer (2020) showed that the crystal surface roughness (from VSI experiments) did not cause any strong hydrodynamic effects near the surface.
3. Our results show that neither flow regimes (affected by cell geometry) nor consideration of the rough sample topography (specific surface area) and the resulting variability in the flow hydrodynamics could explain the experimentally observed dissolution rate spectra when a constant dissolution rate was used. Sensitivity studies showed that this observation also holds true for increased surface roughness.
4. Presence of spatially variable surface reactivity could describe the experimentally observed dissolution rate spectra. This means that the heterogeneity of a crystal surface and the free energy landscape of the surface play an important, if not determining, role for the dissolution rate spectra under the flow and reactivity regimes considered in this study.
5. The impact of surface roughness on flow hydrodynamics was observed to rise with increased reactivity (i.e., acidity) of the injected solution and with increasing injection fluid velocity.

Declaration of Competing Interest

The authors declare that they have no known competing financial interests or personal relationships that could have appeared to influence the work reported in this paper.

ACKNOWLEDGEMENTS

The research work of P.A., M.W. and A.R. is part of the Industrial Partner- ship Programme i32 Computational Sciences for Energy Research that is carried out under an agreement between Shell and the Netherlands Organization for Scientific Research (NWO). M.W. has received funding from the European Research Council (ERC) under the European Union's Horizon 2020 research and innovation programme (grant agreement No. [819588]). The research of O.I. was partially supported from the Bundesministerium für Bildung und Forschung (BMBF), Germany, via project RESKIN, 0310011C. CF and TB gratefully acknowledge funding by the German Federal Ministry of Education and Research (BMBF), grant 02NUK053B and the Helmholtz Association, grant SO-093 (iCross). The authors are thankful for associate editor Carl Steefel and for two reviewers for helpful comments and suggestions in improving this manuscript.

The funding sources had no involvement in study design, collection, analysis and interpretation of data, or in the writing of the report or in the decision to submit the article for publication.

APPENDIX A. SUPPLEMENTARY MATERIAL

Supplementary data to this article can be found online at https://doi.org/10.1016/j.gca.2021.05.003.

REFERENCES

Agrawal P., Raoof A., Iliev O. and Wolthers M. (2020) Evolution of pore-shape and its impact on pore conductivity during CO_2 injection in calcite: Single pore simulations and microfluidic experiments. *Adv. Water Resour.* **136**.

Arvidson R. S., Ertan I. E., Amonette J. E. and Luttge A. (2003) Variation in calcite dissolution rates: A fundamental problem?. *Geochim. Cosmochim. Acta* **67**, 1623–1634.

Bollermann T. and Fischer C. (2020) Temporal evolution of dissolution kinetics of polycrystalline calcite. *Am. J. Sci.* **320**, 53–71.

Brand A. S., Feng P. and Bullard J. W. (2017) Calcite dissolution rate spectra measured by in situ digital holographic microscopy. *Geochim. Cosmochim. Acta* **213**, 317–329.

Busenberg E. and Plummer L. N. (1986) A comparative study of the dissolution and crystal growth kinetics of calcite and aragonite. *Stud. Diagenesis, U.S Geol. Surv. Bull.* **1578**, 139–168.

Chou L., Garrels R. M. and Wollast R. (1989) Comparative study of the kinetics and mechanisms of dissolution of carbonate minerals. *Chem. Geol.* **78**, 269–282.

Deng H., Molins S., Trebotich D., Steefel C. and DePaolo D. (2018) Pore-scale numerical investigation of the impacts of surface roughness: Upscaling of reaction rates in rough fractures. *Geochim. Cosmochim. Acta* **239**, 374–389.

Emmanuel S. and Levenson Y. (2014) Limestone weathering rates accelerated by micron-scale grain detachment. *Geology* **42**, 751–754.

Fischer C., Arvidson R. S. and Lüttge A. (2012) How predictable are dissolution rates of crystalline material?. *Geochim. Cosmochim. Acta* **98**, 177–185.

Fischer C., Kurganskaya I. and Luttge A. (2018) Inherited control of crystal surface reactivity. *Appl. Geochem.* **91**, 140–148.

Gasperino D., Yeckel A., Olmsted B. K., Ward M. D. and Derby J. J. (2006) Mass transfer limitations at crystallizing interfaces in an atomic force microscopy fluid cell: A finite element analysis. *Langmuir* **22**, 6578–6586.

De La Pierre M., Raiteri P., Stack A. G. and Gale J. D. (2017) Uncovering the atomistic mechanism for calcite step growth. *Angew. Chemie - Int. Ed.* **56**, 8464–8467.

Jeschke A. A. and Dreybrodt W. (2002) Dissolution rates of minerals and their relation to surface morphology. *Geochim. Cosmochim. Acta* **66**, 3055–3062.

Kahl W. A., Yuan T., Bollermann T., Bach W. and Fischer C. (2020) Crystal surface reactivity analysis using a combined approach of X-ray micro-computed tomography and vertical scanning interferometry. *Am. J. Sci.* **320**, 27–52.

Kurganskaya I. and Rohlfs R. D. (2020) Atomistic to meso-scale modeling of mineral dissolution: Methods, challenges and prospects. *Am. J. Sci.* **320**, 1–26.

Lasaga A. C. and Luttge A. (2001) Variation of crystal dissolution rate based on a dissolution stepwave model. *Science* **291**, 2400–2404.

Levenson Y. and Emmanuel S. (2013) Pore-scale heterogeneous reaction rates on a dissolving limestone surface. *Geochim. Cosmochim. Acta* **119**, 188–197.

Levenson Y., Schiller M., Kreisserman Y. and Emmanuel S. (2015) Calcite dissolution rates in texturally diverse calcareous rocks. *Geol. Soc. London Spec. Publ.* **406**, 81–94.

Liang Y. and Baer D. R. (1997) Anisotropic dissolution at the CaCO3(1014)-water interface. *Surf. Sci.* **373**, 275–287.

Lüttge A., Winkler U. and Lasaga A. C. (2003) Interferometric study of the dolomite dissolution: A new conceptual model for mineral dissolution. *Geochim. Cosmochim. Acta* **67**, 1099–1116.

Molins S., Soulaine C., Prasianakis N. I., Abbasi A., Poncet P., Ladd A. J. C., Starchenko V., Roman S., Trebotich D., Tchelepi H. A. and Steefel C. I. (2020) Simulation of mineral dissolution at the pore scale with evolving fluid-solid interfaces: review of approaches and benchmark problem set. Comput. Geosci.

Noiriel C. (2015) Resolving time-dependent evolution of pore-scale structure, permeability and reactivity using X-ray microtomography. *Rev. Mineral. Geochem.* **80**, 247–285.

Noiriel C., Oursin M. and Daval D. (2020) Examination of crystal dissolution in 3D: A way to reconcile dissolution rates in the laboratory?. *Geochim. Cosmochim. Acta* **273**, 1–25.

Parkhurst D. and Appelo C. (2013) Description of Input and Examples for PHREEQC Version 3—A Computer Program for Speciation, Batch-Reaction, One-Dimensional Transport, and Inverse Geochemical Calculations.

Peruffo M., Mbogoro M. M., Adobes-Vidal M. and Unwin P. R. (2016) Importance of mass transport and spatially heterogeneous flux processes for in situ atomic force microscopy measurements of crystal growth and dissolution kinetics. *J. Phys. Chem. C* **120**, 12100–12112.

Plummer (1978) The kinetics of calcite dissolution in CO_2-water systems at 5° to 60°C and 0.0 to 1.0 atm CO_2. *Am. J. Sci.* **278**, 179–216.

Plummer L. N. and Busenberg E. (1982) The solubilities of calcite, aragonite, and vaterite in carbon dioxide-water solutions between 0 and 90°C, and an evaluation of the aqueous model for the system calcium carbonate-carbon dioxide-water. *Geochim. Cosmochim. Acta* **46**, 1011–1040.

Pokrovsky O. S., Golubev S. V. and Schott J. (2005) Dissolution kinetics of calcite, dolomite and magnesite at 25 °C and 0 to 50 atm pCO2. *Chem. Geol.* **217**, 239–255.

Shiraki R., Rock P. A. and Casey W. H. (2000) Dissolution kinetics of calcite in 0.1 M NaCl solution at room temperature: An atomic force microscopic (AFM) study. *Aquat. Geochem.* **6**, 87–108.

Sjöberg E. L. and Rickard D. T. (1984) Calcite dissolution kinetics: surface speciation and the origin of the variable pH dependence. *Chem. Geol.* **42**, 119–136.

Steefel C. I., Beckingham L. E. and Landrot G. (2015) Micro-continuum approaches for modeling pore-scale geochemical processes. *Rev. Mineral. Geochemistry* **80**, 217–246.

Wolthers M., Di Tommaso D., Du Z. and De Leeuw N. H. (2012) Calcite surface structure and reactivity: Molecular dynamics simulations and macroscopic surface modelling of the calcite-water interface. *Phys. Chem. Chem. Phys.* **14**, 15145–15157.

Yoon H., Chojnicki K. N. and Martinez M. J. (2019) Pore-scale analysis of calcium carbonate precipitation and dissolution kinetics in a microfluidic device. *Environ. Sci. Technol.* **53**, 14233–14242.

Yoon H., Kang Q. and Valocchi A. J. (2015) Lattice boltzmann-based approaches for pore-scale reactive transport. *Rev. Mineral. Geochem.* **80**, 393–431.

Yoon H., Valocchi A. J., Werth C. J. and Dewers T. (2012) Pore-scale simulation of mixing-induced calcium carbonate precipitation and dissolution in a microfluidic pore network. *Water Resour. Res.* **48**, 1–11.

Yuan K., Starchenko V., Lee S. S., De Andrade V., Gursoy D., Sturchio N. C. and Fenter P. (2019) Mapping three-dimensional dissolution rates of calcite microcrystals: effects of surface curvature and dissolved metal ions. *ACS Earth Sp. Chem.* **3**, 833–843.

Zeebe, R. and Wolf-Gladrow, D. (2001) CO2 in Seawater: Equilibrium, Kinetics, Isotopes, Elsevier Oceanography Book Series, 65, 346 pp, Amsterdam.

Associate editor: Carl Steefel